AIMS Materials Science, 6(1): 111–118.
DOI: 10.3934/matersci.2019.1.111
Received: 16 December 2018
Accepted: 18 February 2019
Published: 20 February 2019

http://www.aimspress.com/journal/Materials

*Research article*

# Molecular dynamics study of mechanical properties of HMX–PS interface

**Zhimin Cao[1,2], Chenhui Xu[1], Caiwei Xiao[2], Wei Liu[2], Jiaohu Huang[2], Wenjun Zong[1], Junjie Zhang[1,*] and Tao Sun[1]**

[1] Center for Precision Engineering, Harbin Institute of Technology, Harbin 150001, China
[2] Institute of Chemical Materials, China Academy of Engineering Physics, Mianyang 421900, China

*** Correspondence:** Email: zhjj505@gmail.com.

**Abstract:** The interface between explosive crystal and binder polymer plays a critical role in the stabilities of energetic materials. In the present work, we investigate the mechanical properties of cyclotetramethylenetetranitramine (HMX)–polystyrene (PS) interface by performing molecular dynamics simulations of uniaxial tension, nanoindentation and nanoscratching tests. Our simulation results indicate that the HMX–PS interface has a mediate strength between HMX of high strength and PS of low strength. In particular for nanoindentation and nanoscratching, the distance of indentation position or scratching position to the HMX–PS interface has a strong influence on mechanical deformation behavior of HMX–PS system. Specifically, the HMX–PS interface has the lowest indentation force and scratching force than both the HMX and the PS.

**Keyword:** energetic materials; HMX–PS; interface stability; molecular dynamics simulation

## 1. Introduction

Energetic materials (EMs) can release high amount of stored chemical energy in a short time under external mechanical, thermal, electrical and shock stimulations, and have been widely used in fields of defense, space and chemistry [1,2]. Safety and security are central topics for the applications of EMs, which require a fundamental investigation of microscopic structural characteristics and their correlation with stabilities of EMs [3].

The explosive crystal of EMs is bound together in a matrix of polymer elastomers to resist unintentional detonation. For instance, the commonly used cyclotetramethylenetetranitramine

(HMX)-based explosive is composed of a HMX crystal bound with amorphous polystyrene (PS). The differences in molecule structure and properties between HMX and PS lead to heterogeneous characteristic of the HMX–PS interface, which plays a critical role in determining the performance of EMs. For instance, An et al. reported that the shear along the nonuniform interface of cyclotrimethylenetrinitramine (RDX)–hydroxyl-terminatedpolybutadiene (HTTP) under shock wave leads to formation of hot-spot due to a large temperature increase, which is also coupled with chemical reaction that leads to detonation [4]. In addition, many studies have been conducted on HMX-based explosives. Duarte et al. established a phase field damage model that includes heat source due to frictional heating at the crack surfaces and heat dissipation in heating processes [5]. Yan et al. studied the electric field changes around different types of defects, such as spherical holes in the interior of energetic materials under the action of laser, and indicated that spherical holes are more likely to generate "hot spots" than cracks and other defects through theory [6]. Barua et al. used finite element analysis method from mesoscopic scale to analyze the thermodynamic response of polymer bonded explosives under impact loading [7–9]. Xiong et al. investigated the binding energy, radial distribution function, X-ray powder diffraction, cohesive energy density and mechanical properties of TKX-50/HMX cocrystal based on molecular dynamics (MD) simulations [10]. Fu et al. performed MD simulations to study the interaction between a HTPE polymer and energetic plasticizers in a solid propellant and their underlying mechanisms [11]. However, previous MD simulation studies of interface properties in EMs mainly focused on the optimized structures of the EMs system, and there is rather limited work reported on the local deformation of the interfaces. Therefore, a fundamental understanding of interface instabilities in EMs is still far from being completed.

The interfacial instabilities are jointly determined by thermal, chemical and mechanical properties of explosive crystals and binder polymers. In particular, mechanical properties of the crystal-binder interface strongly affect the initiation of external stimulation-induced deformation, which subsequently triggers temperature increases along the interface. Therefore, it is of significant importance to investigate mechanical properties of the interface in EMs. While experimental study of EMs is challenging due to the safety issues, MD simulation-based theoretical investigation is a powerful technique for elucidating underlying mechanisms governing the interfacial instabilities [12].

Therefore, in the present work we perform MD simulations to investigate mechanical properties of the HMX–PS interface using the ReaxFF reactive force field. Specifically, MD simulations of uniaxial tension, spherical indentation and scratching tests are conducted to derive mechanical properties of the HMX–PS interface.

## 2. Method

Figure 1 shows the MD model of HMX–PS system, which consists of a crystal HMX and an amorphous PS. Either HMX or PS has a representation of full-atomic resolution. The HMX has a length of 20 nm, a thickness of 5 nm and a width of 7 nm, which contains 60480 atoms. The PS has a length of 24 nm, a thickness of 8 nm and a width of 9 nm, which contains 45080 atoms. The intermolecular and intramolecular interactions in the HMX–PS system are described by the ReaxFF reaction force field [13]. The ReaxFF method implicitly describes chemical bonding without expensive Quantum mechanics calculations by casting the empirical interatomic potential within a bond-order formalism [14].

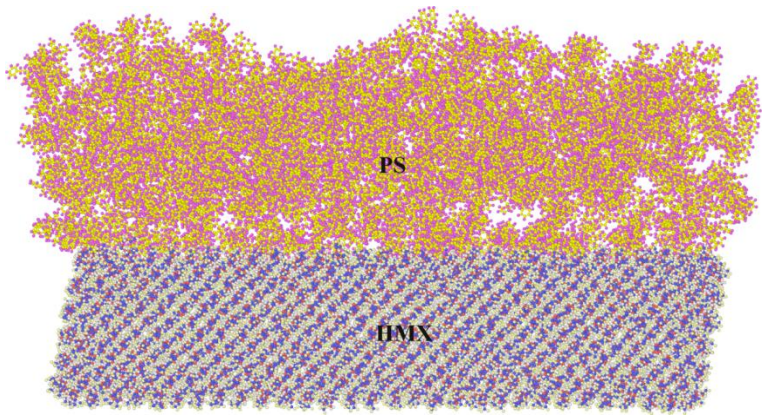


**Figure 1.** MD model of HMX–PS system.

Prior to mechanical tests, the as-constructed HMX–PS system is relaxed to its equilibrium configuration by following procedures: first energy minimization at 0 K, followed by heating to room temperature of 300 K for 10 ps in the canonical NVT ensemble. Figure 1 shows that after relaxation, there are bonding formed between HMX and PS, which leads to formation of a nonuniform HMX–PS interface. Then the equilibrated HMX–PS system is subjected to mechanical tests of uniaxial tension, nanoindentation and nanoscratching. Specifically, the uniaxial tension is performed by deforming the simulation box with a strain rate of $4 \times 10^{11}$/s. The nanoindentation is performed in a displacement-controlled mode with a maximum indentation depth of 1 nm. The spherical indenter with a radius of 1.5 nm has a velocity of 20 m/s. Five indentation positions with equal spacing of 1 nm are selected. Two positions are on the HMX surface, one position is right on the HMX–PS interface, and the other two positions are on the PS surface. After nanoindentation, the indenter scratches the specimen with a constant velocity of 20 m/s along the longitudinal direction while keeping the scratching depth of 1 nm unchanged. The maximum scratching length is 12.5 nm. We note that both utilized strain rate and nanoindentation and nanoscratching velocities are a few magnitudes higher than that used in the experiments, aiming to reduce computational time due to the intrinsic requirement of integration time step of femtosecond in MD simulation. All the MD simulations are conducted within the LAMMPS code [15], and the Ovito [16] is employed to visualize MD data and generate snapshots.

## 3. Results and discussion

### *3.1. Uniaxial tension*

In order to analyze the strength of the HMX–PS interface, uniaxial tension of the HMX–PS system is performed. In addition, uniaxial tension tests of HMX and PS are also performed for comparison purpose. Figure 2a shows the stress–strain curves for the three uniaxial tension tests. Since the HMX–PS system is smaller than the simulation box, the elongation of simulation box is larger than the HMX–PS system. Consequently, the HMX–PS system, as well as PS and HMX have a tensile stress state. Figure 2a demonstrates that the HMX and the PS has the highest and lowest magnitude of stress, respectively, which indicates that HMX has a higher strength than PS. Furthermore, the stress–strain curve of the HMX–PS system is between the curves of HMX and PS,

suggesting a mediate strength of the HMX–PS interface. Figure 2b plots evolutions of temperature with strain for different systems. It is seen from Figure 2b that the increase of temperature is the most pronounced for HMX, followed by HMX–PS, and the least is PS. It is indicated that a higher strength means a higher temperature increase of the system in uniaxial tensile test.

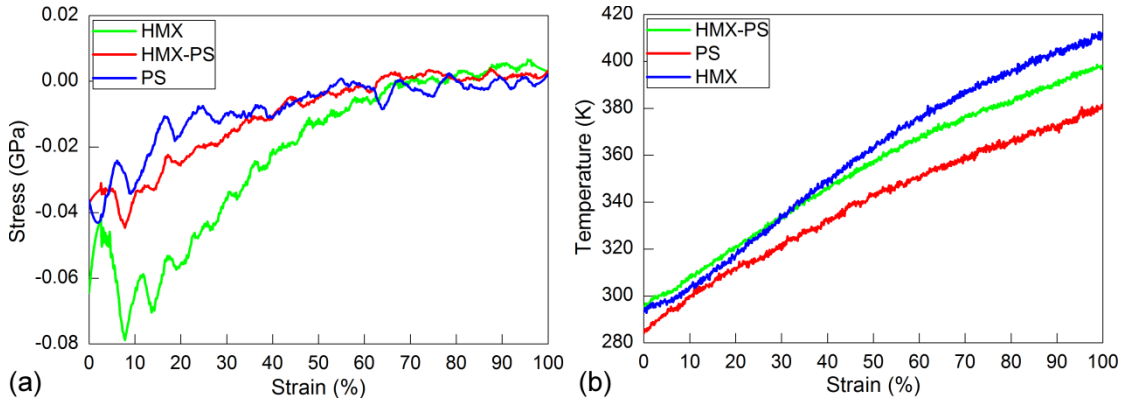


**Figure 2.** Uniaxial tension results: (a) Stress–strain curves; (b) Temperature–strain curves.

Figure 3 presents MD snapshots of different systems before and after tension tests. Figure 3a shows that amorphous PS undergoes significant internal structure change, and the thickness of PS after tension is almost doubled. In contrast, the structural change of HMX is very limited. Interestingly, the structural change of HMX occurs in the middle of the specimen, and the two end sides remain nearly unchanged. For the HMX–PS system, Figure 3b shows that the structural change of both HMX and PS is more pronounced than their single counterparts. More interestingly, the HMX–PS interface is remained unchanged after tension, which leads to the more serious structural change of PS than HMX. Above results indicate that the strength of the HMX–PS interface is dominated by the HMX counterpart. In addition, the structural stability of HMX under mechanical stimulation is higher than that of PS.

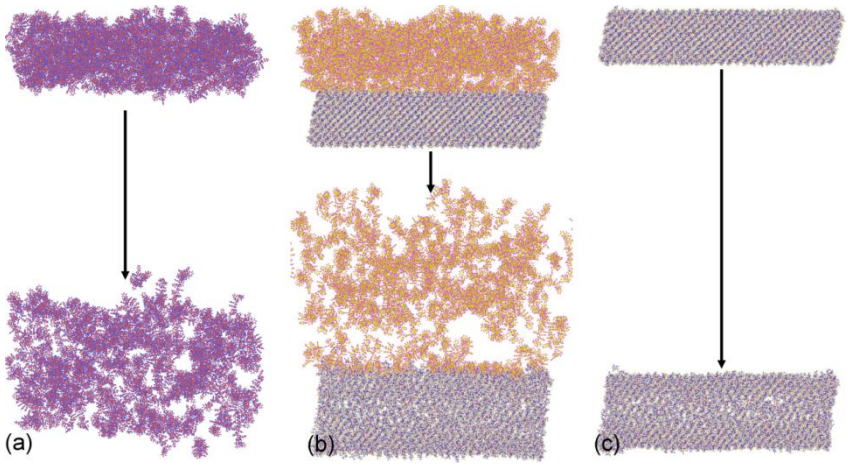


**Figure 3.** MD snapshots (a) PS, (b) HMX–PS and (C) HMX before (top row) and after (bottom row) uniaxial tension. Atoms are colored according to their types.

### *3.2. Nanoindentation*

Series of spherical nanoindentation tests at five different positions along the HMX–PS interface are performed. Figure 4a plots the load–displacement curves for nanoindentation at different positions. It can be seen from Figure 4 that the two load–displacement curves for the nanoindentation on HMX surface basically coincide with each other, indicating that the distance between the indentation position and interface has a negligible influence on mechanical properties of HMX. However, the mechanical properties of PS are strongly affected by the propensity of indentation position to the interface. This can be attributed to that the structure of HMX changes regularly, while the structure of PS is amorphous.

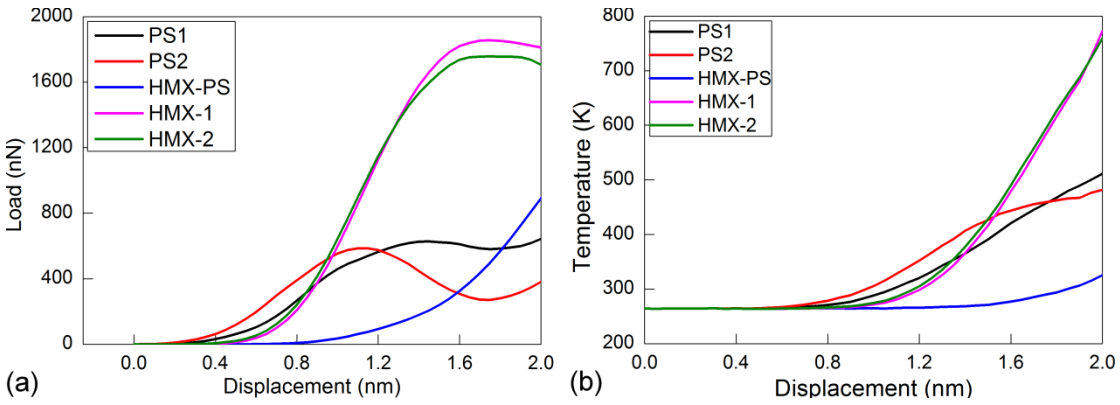


**Figure 4.** Spherical nanoindentation results: (a) Load–displacement curves; (b) Temperature–displacement curves.

In addition, it can be seen from Figure 4a that the indentation force for HMX is less than that for PS when the displacement is less than 1 nm. With a further increase in displacement, however, the indentation force for HMX gradually exceeds that for PS. A careful examination of MD snapshots shows that the molecule structure of PS after relaxation is scattered accompanied with individual chains irregularly residing on surface, while the molecule structure of HMX is still regular. Consequently, the spherical indenter touches individual PS chains first. However, with a further indentation, the spherical indenter fully touches the surface of HMX, which leads to a rapid increase of indentation force on HMX. Therefore, the displacement of the indenter is 2 nm, but the indentation depth is 1 nm. Figure 4a shows that the load-displacement curve for the HMX–PS interface is quite smooth. At the end of nanoindentation the spherical indenter is fully contacted with the HMX and PS, the load is higher than PS but lower than HMX, indicating the mediate strength of the HMX–PS interface.

Figure 4b plots temperature evolutions of HMX–PS system in different nanoindentation tests, indicating similar trends with the evolution of loads, as the increase of temperature in PS is more pronounced than that in HMX in the initial stage, but is reversed when the indenter is fully contacted with chains. Specifically, the increase of temperature in nanoindentation of HMX and PS is independent and dependent on indentation position, respectively. Figure 4b also shows that the temperature increase for indentation on the HMX–PS system is the minimum, indicating that the HMX–PS interface is more energetically stable than HMX and PS.

Figure 5 presents MD snapshots of HMX–PS after nanoindentation. The residual indentation mark on the HMX surface and the HMX–PS interface is clearly visible in Figure 5a,b, respectively. Since the PS has an amorphous structure, the indentation mark cannot be observed clearly. It is seen from Figure 5a that the nanoindentation only leads to local structural change of the HMX crystal. However, the nanoindentation leads to more pronounced structural change in PS, such as intra-chain modification and inter-chain sliding due to the amorphous characteristics of PS structure [17].

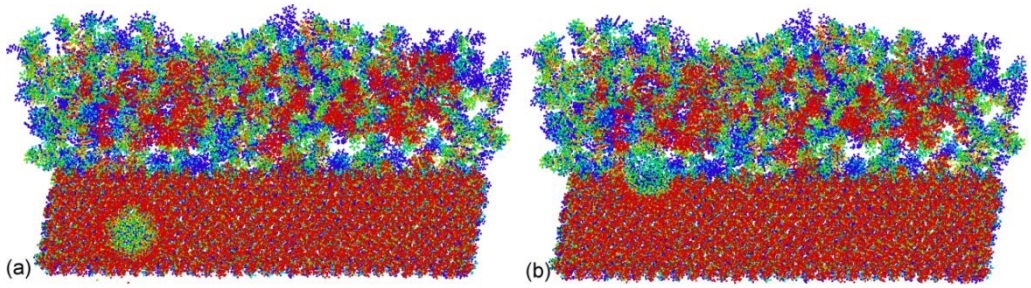


**Figure 5.** MD snapshots of nanoindentation on (a) HMX surface and (b) HMX–PS interface. Atoms are colored according to their heights.

### *3.3. Nanoscratching*

After nanoindentation, subsequent nanoscratching tests along the longitudinal direction are performed. The scratching depth is kept constant as 1 nm. Figure 6 plots evolutions of scratching force with scratching length for different scratching tests. For the scratching on PS, the scratching force generally fluctuates strongly, and goes down to zero for certain period. This is caused by the irregular residing of individual chains. Furthermore, the scratching close to the HMX–PS interface (PS-1) has a higher force than that far from the HMX–PS interface (PS-2). However, the scratching force for HMX is stable after initial run-in period. And the scratching force of HMX is independent on the distance from the HMX–PS interface. For scratching on the HMX–PS interface, the variation of scratching force also shows similar features with PS, but the magnitude is lower than both PS and HMX.

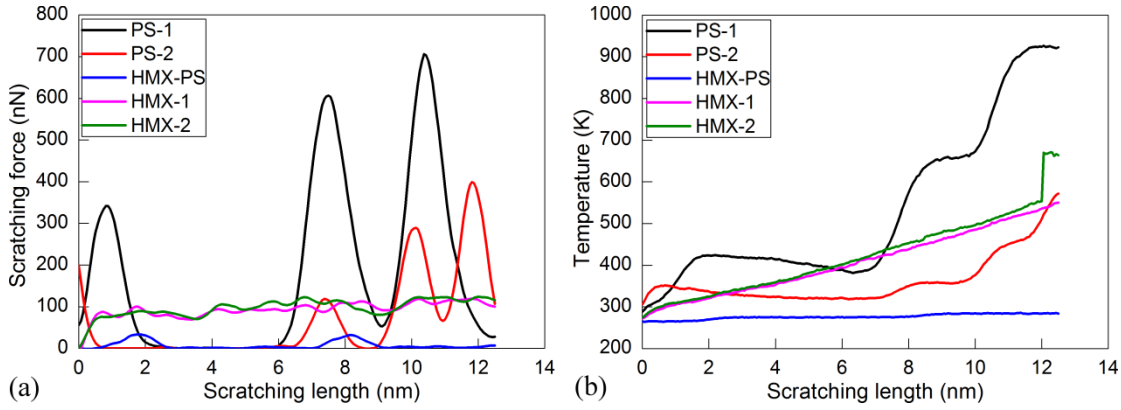


**Figure 6.** Nanoscratching results: (a) Scratching force–scratching length curves; (b) Temperature–scratching length curves.

Figure 6b plots evolutions of temperature with scratching length for the five scratching tests. It is seen that the increase of temperature is synchronized to scratching force. While temperature evolution of PS shows strong fluctuations due to occasional contacts between indenter and individual chains, the temperature of HMX in nanoscratching increases linearly with scratching length, indicating the stability of HMX structure. Figure 6b shows that the increase of temperature in the vicinity of the HMX–PS interface is the minimum.

Figure 7 presents MD snapshots of the HMX–PS system after nanoscratching. The scratching-induced wear scar is clearly visible on the HMX surface, as shown in Figure 7. However, the wear scar cannot be observed for nanoscratching on both the HMX–PS interface and the PS surface, because of the occasional contacts between indenter and individual chains. It suggests that the deformation behavior of the HMX–PS system can be greatly influenced by the amorphous PS, due to the energetically favored interchain sliding.

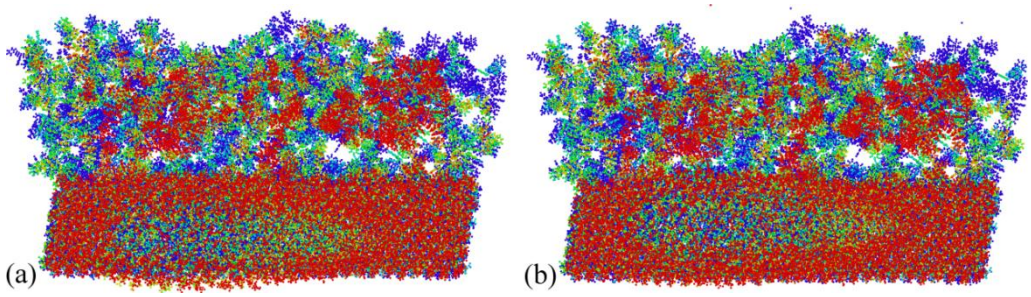


**Figure 7.** MD snapshots of nanoscratching (a) HMX-1 and (b) HMX-2. Atoms are colored according to their heights.

## 4. Conclusion

In the present work, we perform MD simulations of uniaxial tension, nanoindentation and nanoscratching tests to investigate mechanical properties of the HMX–PS interface. The strength of the HMX–PS interface is the mediate between HMX and PS, which also leads to mediate temperature increasing. The HMX–PS interface is more stable with less structural evolution than both HMX and PS. For nanoindentation and nanoscratching, the mechanical response and deformation behavior of the HMX–PS system are strongly influenced by the distance of indentation and scratching from the HMX–PS interface. And the increases in load and temperature are the minimum for the HMX–PS interface.

## Acknowledgement

The authors greatly acknowledge support from the National Natural Science Foundation of China (51505441).

## Conflict of interest

The authors declare that they have no conflict of interest.

## References


1. Mathieu D (2017) Sensitivity of energetic materials: Theoretical relationships to detonation performance and molecular structure. *Ind Eng Chem Res* 56: 8191–8201.
2. Zhang JH, Shreeve JM (2016) Time for pairing: cocrystals as advanced energetic materials. *CrystEngComm* 18: 6124–6133.
3. Maienschein J, Pantoya M (2014) Safety in energetic materials research and development—approaches in academia and a national laboratory. *Propell Explos Pyrot* 39: 483–485.
4. An Q, Zybin SV, Goddard III WA, et al. (2011) Elucidation of the dynamics for hot-spot initiation at nonuniform interfaces of highly shocked materials. *Phys Rev B* 84: 220101.
5. Duarte CA, Grilli N, Koslowski M (2018) Effect of initial damage variability on hot-spot nucleation in energetic materials. *J Appl Phys* 124: 025104.
6. Peng YJ, Ye YQ (2015) Research progress of 'Hot-Spot' theory in energetic materials initiation. *Chemistry* 78: 693–701.
7. Barua A, Zhou M (2011) A lagrangian framework for analyzing microstructural level response of polymer-bonded explosives. *Model Simul Mater Sc* 19: 055001.
8. Barua A, Horie Y, Zhou M (2012) Energy localization in HMX-Estane polymer-bonded explosives during impact loading. *J Appl Phys* 111: 054902.
9. Barua A, Zhou M (2013) Computational analysis of temperature rises in microstructures of HMX-Estane PBXs. *Comput Mech* 52: 151–159.
10. Xiong S, Chen S, Jin S, et al. (2017) Molecular dynamic simulations on TKX-50/HMX cocrystal. *RSC Adv* 7: 6795–6799.
11. Fu X, Fan X, Ju X, et al. (2015) Molecular dynamic simulations on the interaction between an HTPE polymer and energetic plasticizers in a solid propellant. *RSC Adv* 5: 52844–52851.
12. Yuan DD, Zhu PZ, Fang FZ, et al. (2013) Study of nanoscratching of polymers by using molecular dynamics simulations. *Sci China Phys Mech Astron* 56: 1760–1769.
13. Chenoweth K, Van Duin ACT, Goddard WA (2008) ReaxFF reactive force field for molecular dynamics simulations of hydrocarbon oxidation. *J Phys Chem A* 112: 1040–1053.
14. Senftle TP, Hong S, Islam MM, et al. (2016) The ReaxFF reactive force-field: development, applications and future directions. *npj Comput Mater* 2: 15011.
15. Plimpton S (1995) Fast parallel algorithms for short-range molecular dynamics. *J Comput Phys* 117: 1–19.
16. Stukowski A (2010) Visualization and analysis of atomistic simulation data with OVITO—the Open Visualization Tool. *Model Simul Mater Sc* 18: 015012.
17. Du K, Tang Y, Zhang J, et al. (2013) Velocity-dependent nanoscratching of amorphous polystyrene. *Curr Nanosci* 9: 153–158.



AIMS Press